CHEMISTRY OF MATERIALS

Article

pubs.acs.org/cm

Effects of Substituents on Transport Properties of Molecular Materials for Organic Solar Cells: A Theoretical Investigation

Domenico Alberga,[†] Ilaria Ciofini,[†] Giuseppe Felice Mangiatordi,[‡] Alfonso Pedone,[§] Gianluca Lattanzi,[∥] Jean Roncali,*[,⊥] and Carlo Adamo*[,†]

[†]Institut de Recherche de Chimie Paris CNRS Chimie ParisTech, PSL Research University, 11 rue P. et M. Curie, F-75005 Paris 05, France

[‡]Dipartimento di Farmacia-Scienze del Farmaco, Università di Bari "Aldo Moro", Via Orabona, 4, I-70126 Bari, Italy

[§]Department of Chemical and Geological Sciences, University of Modena and Reggio Emilia, Via Campi 103, 41125 Modena, Italy

[∥]Dipartimento di Fisica, Università di Trento, Via Sommarive 14, 38123 Povo-Trento, Italy

[⊥]Group Linear Conjugated Systems, CNRS UMR 6200, Moltech-Anjou, University of Angers, 2 Bd Lavoisier, 49045 Angers, France

Supporting Information

ABSTRACT: We present a theoretical investigation of the effects of substitution of the triphenylamine (TPA) block on the overall properties of materials based on small push−pull molecules designed as donors for organic photovoltaics (OPV). In particular, we exploit modern computational techniques such as density functional theory (DFT), time-dependent DFT, molecular dynamics, and the Marcus theory to analyze the charge and exciton transport properties in crystalline and amorphous phases of four compounds in which one phenyl ring of the TPA block of 2-[(5-{4-[methyl-(phenyl)amino]phenyl}thiophen-2-yl)methylene]-malononitrile is replaced with a methyl, an α-naphthyl, and a β-naphthyl. Our calculations unveil the molecular rationale behind the different transport properties observed in the experiments. We show that, although the effects of the substituents on the electronic and optical properties are negligible, they have an impact on the molecular packing of the crystalline structure, thus explaining the different macroscopic transport properties (observed and calculated). In particular, the substitution of a phenyl with a methyl favors face-to-face $\pi-\pi$ packing in the crystal structure and allows a good π-orbital overlap and high hopping rates. On the other hand, the introduction of an α-naphthyl group generates a steric hindrance that negatively affects the transport properties. Moreover, the investigated substitutions do not significantly influence the degree of local order in the amorphous bulks displaying complete disorder and low hole mobilities. These results, in agreement with the experimental findings, suggest that our computational approach is able to account for the macroscopic effect of subtle transformations of a molecular structure on transport properties and thus can be further employed to obtain valuable insights into the molecular design of optimized active materials for OPV.

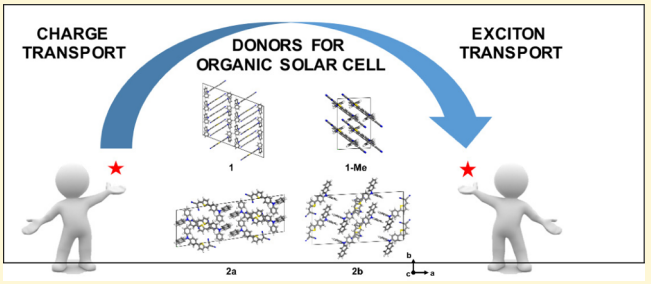

INTRODUCTION

Organic photovoltaics (OPV) are attracting increasing amounts of interest as an alternative to inorganic solar cells because of their possible applications in low-cost, low-environmental impact, lightweight, and large-area flexible devices.[1−4] An organic solar cell (OSC) basically consists of the heterojunction created by contacting an electron donor material (D) with an electron acceptor (A).[5] The basic functioning of an OSC consists of four steps. The absorption of an incident photon by the active material (D in general) generates a bound electron−hole pair (exciton) that diffuses in the D phase and dissociates at the D−A interface. The resulting electrons and holes migrate in the D and A layers to be collected during the last step at the electrodes.[1,2]

The performance of an OSC depends on the efficiency of these four steps that is affected, in turn, by the properties of the materials employed in its fabrication. Its optimal performance requires an improvement of the characteristics of each constituent.[6]

OSCs can be roughly dived into two main categories: bilayer planar heterojunctions (PHJs) essentially fabricated by vacuum deposition techniques[7,8] and bulk heterojunction solar cells (BHJs) in which the heterojunction created at the interface of segregated phases of donor and acceptor materials is distributed in the entire volume of a solution-processed active film. Besides fabrication by solution processes at room temperature, BHJs have an advantage of a large increase of the area of the D−A interface and thus exhibit better efficiency.[9,10] Whereas soluble

Received: October 7, 2016
Revised: November 27, 2016
Published: December 5, 2016

DOI: 10.1021/acs.chemmater.6b04277
Chem. Mater. XXXX, XXX, XXX−XXX

conjugated polymers have represented the major class of donor materials for solution-processed BHJs for more than 20 years,[11] molecular donors have recently emerged on the forefront of research on the chemistry of OPV materials due to the advantages of well-defined chemical structures in terms of the reproducibility of synthesis and purification and possible analyses of structure−property relationships.[12−16] Because of a multidisciplinary research effort focused on both the optimization of cell fabrication and the synthesis of new donor materials, conversion efficiencies comparable to those obtained with the best polymer-based cells (>10%) have recently been reported for BHJ cells based on molecular donors with relatively complex chemical structures.[17] Besides a high conversion efficiency, the future industrial development of OPV depends on the possibility of offering decisive economic and environmental advantages over existing technologies. In this context, the development of active materials combining simple, cost-effective, clean, and scalable synthesis represents a key issue for the chemistry of OPV materials.[18]

In this work, we focus on the donor materials. In particular, an efficient donor material for OPV must combine[19] (1) good light harvesting properties, namely, an absorption spectrum covering a large part of the solar irradiation spectrum and a high molecular extinction coefficient; (2) high hole mobility and a high exciton diffusion coefficient to minimize the transport resistance in the bulk; (3) a large delocalization of the highest occupied molecular orbital (HOMO) that facilitates hole transport; (4) a low HOMO energy level that increases the open circuit voltage (V_{oc}) of the solar cell; and (5) a high exciton diffusion coefficient and a low exciton binding energy facilitating exciton dissociation at the donor−acceptor interface.

A typical strategy employed to propose novel and better performing molecules consists of optimizing a reference skeleton with substituent groups that would enhance its charge and exciton transport properties.[20−22] The structural change of the molecular scaffold is aimed at optimizing the relevant photovoltaic parameters of solar cells adopting these donor materials.

Recently, small triarylamine-based (TAA) donor molecules have exhibited interesting photovoltaic performances.[14,16,23,24] The number of TAA-based molecules studied within this context is huge, thus showing the fervent experimental interest in this subject.[25−27] Because of a combination of electron donor properties and high hole mobility, TAAs represent a major class of key building blocks for the design of metal-free chromophores for dye-sensitized solar cells[28,29] and donor materials for OPV.[12−16,21,30−32] Much work has already been devoted to the analysis of structure−property relationships in TAA-based molecular donors for OPV, and in particular, recent results for push−pull systems have shown that replacement of phenyl groups of the triphenylamine (TPA) block with some aromatic or aliphatic substituents has a negligible impact on the electronic properties of the molecule but can induce dramatic changes in the charge transport properties of the resulting materials. In particular, replacing an outer phenyl group of compound 2-[(5-{4-[methyl(phenyl)amino]phenyl}thiophen-2-yl)methylene]malononitrile (**1**)[33] with a methyl group (**1-Me**) or the α-naphthyl group of **2a** with a β-naphthyl (**2b**) (Figure 1) leads to a significant increase in hole mobility and photovoltaic conversion efficiency.[32,34]

In this context, computational techniques represent a powerful tool that allows us to understand, at an atomistic scale, the physical phenomena that lie behind the transport properties that unveil the structure−property relationship in this class of molecules.[22,35,36]

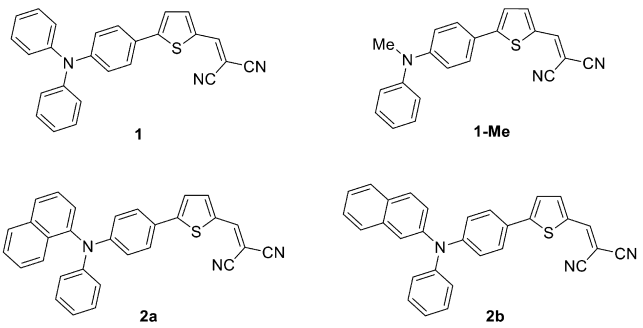

Figure 1. Chemical structures of the four TAA-based donor materials studied in this work.

Theoretical studies based on classical molecular dynamics (MD) and quantum chemical calculations were recently employed to fully characterize the structural, electronic, optical, and transport properties of organic semiconductors in solar cells.[35−41] Charge and exciton transport in organic semiconductors are commonly described as a hopping process whose rate can be derived from the Marcus theory.[42] This technique can be successfully used to calculate the charge mobility, or the exciton diffusion coefficient, employing a master equation or the kinetic Monte Carlo (KMC) approach.[43,44] The quantities entering the Marcus rates can be calculated using the most appropriate level of theory depending on the complexity of the studied system. In this context, it has been shown that Marcus rate calculations based on the use of a semiempirical Hamiltonian (ZINDO) produce reliable results that can be compared to the experimental values. This technique is thus suitable for studying transport on large scales or complex systems.[45,46] Not surprisingly, this approach was successfully applied to the study of hole transport in molecular and polymeric systems using configurations extracted from MD simulations in the amorphous phase.[36,39,47−49]

Framed in this picture, our study aims to investigate the four recently proposed TAA molecules[32−34] depicted in Figure 1. We apply a modern computational approach involving classical and quantum calculations and exploiting the Marcus theory to shed light on the structure−property relationship that rules charge and exciton transport in these systems in both crystalline and amorphous phases.

The paper is structured as follows. After a description of the employed computational protocol, the calculated transport properties of the four investigated materials are discussed in terms of their electronic, optical, and packing properties. The results are presented with the perspective of providing valuable insights into the rational design of new and better performing molecules.

COMPUTATIONAL METHODS

The crystal structures of molecules **2a** and **2b** were obtained following the approach described in ref 35, by using the polymorph predictor module in Materials Studio.[50] A single molecule was optimized using the DMol3 module, while electrostatic potential charges of all atoms were obtained employing the PBE functional.[51] Crystal structure prediction was thus conducted using the Dreiding force field,[52] considered the most reliable force field for molecular crystal prediction.[53] The polymorph predictor calculations were restricted to the five most probable space groups, i.e., $P2_1/C$, $P1$, $P212121$, $P21$,

DOI: 10.1021/acs.chemmater.6b04277
Chem. Mater. XXXX, XXX, XXX−XXX

Table 1. Cell Parameters of the Predicted Crystalline Structure of 2a and 2b and Experimental Values of 1[33] and 1-Me[32] (angles in degrees and cell parameters in angstroms)

system	α	β	γ	a	b	c
1[a]	90.0000	90.0000	110.6000	19.8370	15.6120	7.1912
1-Me[b]	82.5470	84.1080	87.1230	5.7003	8.7382	17.5060
2a	67.6937	73.3101	76.4538	23.2413	8.1118	7.9374
2b	54.9466	82.2253	83.2363	19.1165	12.3813	7.1568

[a]Experimental values are taken from ref 33. [b]Experimental values are taken from ref 32.

and $P\bar{1}$.[54] We sorted the obtained crystal structures as a function of their total energies and selected those with the lowest energies.

MD simulations of the amorphous bulk[55] were performed for each compound to calculate the associated hole mobilities. Each system was built starting from a configuration in which 1000 molecules were placed at random positions in a cubic periodic box having an edge of 250 Å. All systems were equilibrated in the *NPT* ensemble at atmospheric pressure and high temperature (P = 1 atm; T = 800 K) until the volume of the periodic box reached an equilibrium value. Following a further equilibration run at 300 K, a 30 ns long trajectory in the *NPT* ensemble was obtained for each system. All MD simulations employed a time step of 1 fs. A cutoff of 12 Å was applied to the van der Waals interactions through a switching function, whereas the particle mesh Ewald (PME) method was employed to calculate the electrostatic interactions. The simulations were performed using the NAMD2.11 package[56] and the CGenFF force field.[57,58] For all considered systems, the restrained electrostatic potential (RESP) procedure[59] was employed to obtain accurate partial charges [based on HF/6-31G(d,p) results]. The equilibrium condition was ensured by verifying that the volume fluctuated around its average value: the plot of the volume of the simulation cell in the 30 ns long *NPT* production run shows that the volume is at equilibrium in all four cases (data in Figure S1).

To simulate the hole transport in each of the four systems in crystalline and amorphous phase, we applied the nonadiabatic high-temperature limit of the semiclassical Marcus charge-transfer theory.[42] This theory is based on the assumption that charges are localized on a single molecule and charge-transfer reactions take place via a hopping mechanism according to which the hopping rate between two molecules, i and j, can be computed as

$$\omega_{ij} = \frac{J_{ij}^2}{\hbar}\sqrt{\frac{\pi}{\lambda k_B T}}\exp\left[-\frac{(\Delta E_{ij}-\lambda)^2}{4\lambda k_B T}\right] \quad (1)$$

where T is the temperature, J_{ij} is the electronic coupling element (or transfer integral) between i and j, $\Delta E_{ij} = E_i - E_j$ is the site energy difference, and λ is the reorganization energy.[42]

The reorganization energy is defined as

$$\lambda = E_{nC} - E_{nN} + E_{cN} - E_{cC} \quad (2)$$

where E_{nN} (E_{cC}) is the electronic energy of the neutral (charged) molecule in its optimized neutral (charged) geometry and E_{nC} (E_{cN}) is the energy of the neutral (charged) molecule in the optimized charged (neutral) geometry. For the four molecules, λ was calculated employing density functional theory (DFT) at the B3LYP/6-311g(d,p) level of theory.

The electronic coupling elements were calculated following the approach presented in ref 46. The latter assumes that the HOMO orbital of a dimer results exclusively from the interaction of the HOMO orbitals ϕ_i and ϕ_j of monomers i and j, respectively, and thus, it can be expanded in terms of those. Within this approach, $J_{ij} = \langle\phi_i|\hat{H}|\phi_j\rangle$, where $\hat{H}$ is the dimer Hamiltonian. All J_{ij} values were calculated using the semiempirical ZINDO method.[45,60]

J_{ij} values were calculated using the semiempirical ZINDO method.[45,60] It has been shown that the ZINDO Hamiltonian produces reliable results comparable to the experimental values. This technique is thus suitable for studying transport in large scale or complex systems.[45,46]

The site energy difference contains three contributions: (1) the internal site energy difference ($\varepsilon_i - \varepsilon_j$), (2) the electrostatic site energy difference calculated within a given volume around the pair using partial charges generated via the Merz–Singh–Kollman scheme,[61] and (3) the contributions of an applied external electric field $\vec{E}$ ($\Delta E_{ext} = -e\vec{E}\cdot\vec{r}_{ij}$, where $\vec{r}_{ij}$ is the vector joining the centers of mass of two molecules.

We calculated the Marcus rates for each molecular pair ij from a neighbor list built with a cutoff of 15 Å. In the case of molecular crystals, we neglected the internal and electrostatic contributions to the site energy difference due to the symmetry of the crystalline phase. For the calculation of the charge mobility in the amorphous phase, we used molecular configurations extracted from MD simulations.

Finally, we calculated the hole mobilities (μ) setting up KMC simulations using the obtained rates. The mobility in the direction of the applied external electric field was calculated as

$$\mu = \frac{\langle v\rangle}{E} \quad (3)$$

where $\langle v\rangle$ is the average velocity of the charge in the direction of the applied field $\vec{E}$.

The exciton diffusion coefficients (D) for the four investigated systems in the crystalline phase were calculated following the approach described in ref 44. Like charge transport, exciton transport can be depicted as a hopping process with a hopping rate described by eq 1. In this case, reorganization energy λ is defined as[62−64]

$$\lambda = E_{nX} - E_{nN} + E_{xN} - E_{xX} \quad (4)$$

where E_{nN} (E_{xX}) is the electronic energy of the molecule in the ground (excited) state of its optimized ground (excited) state geometry and E_{nX} (E_{xN}) is the energy of the molecule in the ground (excited) state of the optimized excited (ground) state geometry. For the four molecules, λ was calculated with DFT calculations optimizing the ground and excited state geometries at the CAM-B3LYP/6-311G(d,p) level and calculating the four terms in eq 4 at the B3LYP/6-311G(d,p) level of theory through single-point calculations.

The excitonic couplings (J_{ij}) are defined as[44,65,66]

$$J_{ij} = \frac{E_{Dim(2)} - E_{Dim(1)}}{2} \quad (5)$$

where $E_{Dim(1)}$ and $E_{Dim(2)}$ are the energies of the two lowest excited states of the dimer resulting from the Davydov splitting[67] of the monomer S_1 levels computed at the CAM-B3LYP/6-311G(d,p) level of theory.

The site energy difference contains only one term derived from the application of a small fictitious drift force $\vec{F}$ ($\Delta E_{ij} = \vec{F}\cdot\vec{r}_{ij}$). This term was introduced in ref 44: the calculations of the exciton diffusion coefficient by means of a simple diffusion rate equation based on the hopping rates and the squared hopping distance possibly lead to an overestimation of the diffusion constant.[65] To overcome this issue, the authors suggest to apply a small fictitious force $\vec{F}$ as a drift term to evaluate an "exciton mobility" in analogy with the charge mobility. The latter, combined with the Einstein relation, leads to

$$D = k_B T\frac{\langle v\rangle}{F} \quad (6)$$

DOI: 10.1021/acs.chemmater.6b04277
Chem. Mater. XXXX, XXX, XXX−XXX

where $\langle v \rangle$ is the average velocity of the exciton in the direction of $\vec{F}$. As in the calculation of hole mobility, D was calculated by means of KMC simulations using the obtained rates.

In our charge and exciton transport models, we neglected recombination phenomena assuming the same recombination rates for all the studied materials.

In the following, DFT-based quantities calculated in implicit solvent are computed using the polarizable continuum model (PCM) approach.[68]

RESULTS AND DISCUSSION

To calculate the hole mobility and the exciton diffusion coefficient in the investigated systems in both crystalline and amorphous phases, we first predicted the crystal structure of molecules **1**, **2a**, and **2b** using Material Studio and the procedure described in Computational Methods. All the obtained structures belong to the same space group ($P\bar{1}$) as the experimentally available crystal structure of molecule **1-Me**.[32] Table 1 reports the predicted cell parameters for the four crystals depicted in Figure 2.

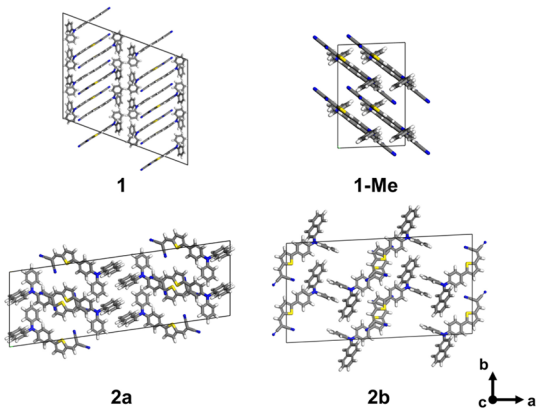

Figure 2. Supercells (2 × 2 × 2) of the predicted crystalline structures of **2a** and **2b** and of the experimental structures of **1-Me**[32] and **1**.[33]

In conjugated molecules, the $\pi-\pi$ packing mode of the dimers inside the crystals plays an important role in determining the hole mobility. In general, configurations characterized by a cofacial $\pi-\pi$ packing allow an optimal π-orbital overlap that in turn ensures relatively large transfer integrals.[35] A first qualitative inspection of the crystals shows that among all molecules, **1-Me** and **2b** have the best geometrical packing that favors face-to-face $\pi-\pi$ stacking, thus enhancing the transport properties.

Using the obtained crystal structures, we calculated the hole mobilities and the exciton diffusion coefficients of supercells (3 × 3 × 5 for **1**, 5 × 5 × 3 for **1-Me**, and 3 × 5 × 5 for the others) along the three crystal axes (μ_a, μ_b, and μ_c) as described in Computational Methods. For the calculation of the hole mobility, we applied an electric field of 10^6 V/m. This value is typical in experimental measurements of charge mobility performed through the time-of-flight (TOF) technique.[60,69] The results along with the average mobilities calculated in the three directions (μ_{av}) and the available experimental values (μ_{exp}) are reported in Table 2.

The calculated μ_{av} values show the same trend as the experimentally observed hole motilities, thus supporting the robustness of our calculation protocol.

For the calculation of the exciton diffusion coefficients of the four crystalline systems, we employed a force of 16 aN in eq 1 as in ref 44. The calculated values in the direction of the three crystal axes (D_a, D_b, and D_c) and the average values (D_{av}) are reported in Table 3.

The calculated D_{av} coefficients are similar for the four systems. In particular, **1-Me** shows a slightly higher value that is in agreement with the highest power conversion efficiency (PCE) measured in solar cells making use of these molecules.[32,34]

On the other hand, it is difficult to find a direct connection between the different transport properties calculated and the chemical structure of the analyzed molecules. First, the differences in both charges and excitonic reorganization energies reported in Tables 2 and 3, respectively, are too small to justify our results. Moreover, and to some extent unexpectedly, the molecule with the highest λ for hole transport, that is **1-Me**, also displays the highest hole mobility. The rationale that lies behind the different transport properties thus has to be found elsewhere.

At first, we looked for possible differences in the electronic and optical properties of the four molecules. Figure 3 shows the HOMO and LUMO orbitals computed for all systems.

It is clear that there is only a trifling difference in the frontier molecular orbitals among the molecules and that the influence of the substituents in the triphenylamine unit on the overall electronic structure is negligible. Moreover, we calculated [at the B3LYP/6-311G(d,p) level] other relevant parameters that depend on the electronic structure of the investigated molecules and can influence the performance of a solar cell, namely, the HOMO−LUMO gap (Δ_{H-L}), the adiabatic ionization potential (IP), and the degree of charge delocalization (D_{chg}) defined as the ratio of the number of atoms of the molecule in the cationic state carrying a partial charge larger than 0.1e to the total number of atoms (Table 4).[36]

The results are in qualitative agreement with the experimental values reported in refs 32 and 34. However, there are no appreciable differences among the studied systems except for **1-Me**: the substitution of an aromatic ring of the triphenylamine unit with a methyl group slightly increases both the Δ_{H-L} and the IP. Apart from that, the substituents in the triphenylamine unit have an only negligible effect on the electronic properties of the HTMs.

Table 2. Experimental (μ_{exp}) and Calculated Hole Mobilities along the Three Crystallographic Axes (μ_a, μ_b, and μ_c) and Their Averages (μ_{av}) (in square centimeters per volt per second)[a]

system	μ_a	μ_b	μ_c	μ_{av}	μ_{exp}[b]	λ
1	2.52×10^{-5}	7.50×10^{-5}	1.14×10^{-4}	7.14×10^{-5}	1.00×10^{-5}	127
1-Me	6.03×10^{-4}	2.45×10^{-4}	4.77×10^{-4}	4.42×10^{-4}	5.00×10^{-4}	194
2a	1.17×10^{-5}	1.03×10^{-5}	8.76×10^{-6}	1.03×10^{-5}	4.20×10^{-6}	156
2b	1.68×10^{-4}	1.14×10^{-4}	1.09×10^{-4}	1.30×10^{-4}	5.50×10^{-5}	120

[a]Computed reorganization energies (λ) are given in millielectronvolts. [b]Experimental values from refs 32 and 34.

DOI: 10.1021/acs.chemmater.6b04277
Chem. Mater. XXXX, XXX, XXX−XXX

Table 3. Exciton Diffusion Coefficients Calculated along the Three Crystallographic Axes (D_a, D_b, and D_c) and the Average Values (D_{av}) (in square meters per second)[a]

system	D_a	D_b	D_c	D_{av}	λ
1	2.18×10^{-5}	2.94×10^{-5}	4.17×10^{-5}	3.10×10^{-5}	119
1-Me	6.94×10^{-5}	1.93×10^{-5}	1.88×10^{-5}	3.58×10^{-5}	128
2a	4.26×10^{-5}	2.86×10^{-5}	1.96×10^{-5}	3.03×10^{-5}	142
2b	4.22×10^{-6}	1.77×10^{-5}	2.95×10^{-5}	1.71×10^{-5}	138

[a]Computed reorganization energies (λ) are given in millielectronvolts.

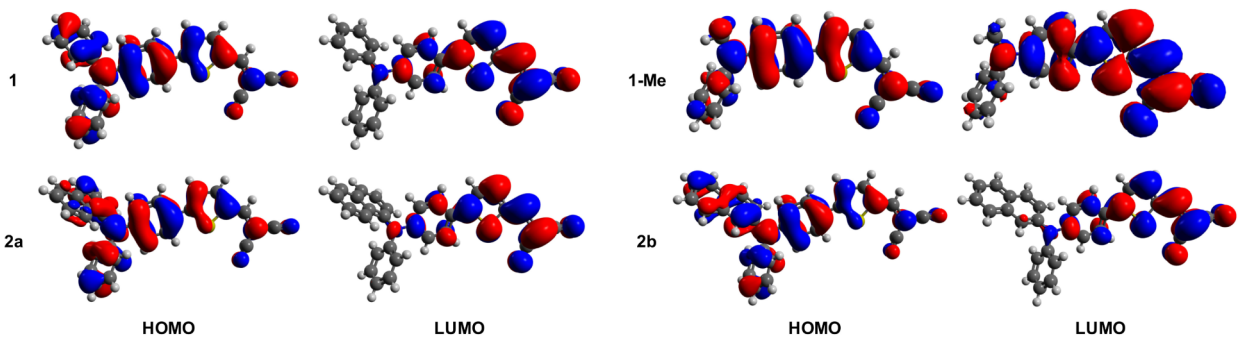

Figure 3. Computed HOMO and LUMO orbitals of the four investigated molecules calculated at the B3LYP/6-311G(d,p) level of theory.

Table 4. Energies of the HOMO and LUMO Orbitals (E_H and E_L, respectively) Calculated at the B3LYP/6- 311G(d,p) Level, HOMO−LUMO Gaps (Δ_{H-L}), Adiabatic Ionization Potentials (IPs) (in electronvolts), and Degrees of Charge Delocalization

system	E_H	E_L	Δ_{H-L}	IP	D_{chg}
1	−5.57	−2.96	2.61	6.66	0.51
1-Me	−5.62	−2.84	2.77	6.77	0.52
2a	−5.58	−2.94	2.63	6.61	0.51
2b	−5.54	−2.97	2.57	6.57	0.52

It might be argued that the systems could differ in their optical properties. To test this hypothesis, we computed the absorption (λ_{abs}) and emission wavelengths (λ_{em}) and their difference (Stoke shift), at the TD-B3LYP/6-311G(d,p) level of theory. Their values are reported in Table 5, along with the optical gap, defined as the first singlet excitation energy, E_1,[70] and the exciton binding energy, E_b. The latter represents the energy required to fully separate the electron−hole pair against Coulomb attraction: it is defined as the energy difference between the neutral exciton and the two free charge carriers (i.e., the electron and the hole). This quantity is expressed as $E_b = E_g - E_1 = \Delta_{H-L} - E_1$. E_g is the electronic band gap, here replaced by the HOMO−LUMO energy gap (Δ_{H-L}).

Table 5. Optical Properties Calculated at the TD-B3LYP/6-311G(d,p) Level of Theory in Implicit Dichloromethane (polarizable continuum model approach[68]), Including Absorption and Emission Wavelengths (λ_{abs} and λ_{em}, respectively) Based on S_0 and S_1 States, Stokes Shifts (in nanometers), First Singlet Excitation Energies (E_1), and Exciton Binding Energies (E_b, in electronvolts)

system	λ_{abs}	λ_{em}	Stoke shift	E_1	E_b
1	552	580	27	2.24	0.29
1-Me	515	540	25	2.40	0.25
2a	544	585	41	2.27	0.30
2b	559	590	31	2.21	0.29

1, **2a**, and **2b** share analogous optical properties, but in **1-Me**, the substitution of an aromatic ring of the triphenylamine unit with a methyl leads to a blue shift in both emission and absorption. Moreover, there is a slight decrease in the exciton binding energy (E_b), which indicates that the electron−hole separation is favored in **1-Me**, thus improving the performance of the solar cell.

Again, these small changes observed for the electronic and optical features of the four molecules cannot justify overall their difference in transport properties. These latter values can thus be ascribed only to the different molecular packing in their crystalline phases induced by the small modifications in their molecular skeleton. Table 6 reports the centroid-to-centroid distances (r_{ij}), the squares of the electronic coupling elements [$J_{ij}^{2(hole)}$ and $J_{ij}^{2(ex)}$] and the hopping rates [$\omega_{ij}^{(hole)}$ and $\omega_{ij}^{(ex)}$] computed for the main hopping pathways for hole and exciton transport in the four systems shown in Figure 4.

Table 6. Centroid-to-Centroid Distances (r_{ij}, in angstroms), Squares of the Electronic Coupling Elements [$J_{ij}^{2(hole)}$ and $J_{ij}^{2(ex)}$ in square millielectronvolts], and Hopping Rates [$\omega_{ij}^{(hole)}$ and $\omega_{ij}^{(ex)}$ in inverse seconds] of the Main Hopping Pathway of Hole and Exciton Transport in the Investigated Systems

system	r_{ij}	$J_{ij}^{2(hole)}$	$\omega_{ij}^{(hole)}$	$J_{ij}^{2(ex)}$	$\omega_{ij}^{(ex)}$
1	8.39	1.97	1.74×10^{13}	95.5	1.98×10^{14}
1-Me	5.70	7.37	4.31×10^{13}	146.3	2.92×10^{14}
2a	13.43	0.11	1.03×10^{12}	117.5	1.56×10^{14}
2b	10.86	2.28	3.62×10^{13}	66.1	5.19×10^{13}

It is clear that among the investigated molecules **2b** and, especially, **1-Me** achieve the best packing in the molecular crystal. In particular, the substitution of the phenyl with a methyl in **1-Me** enhances the face-to-face $\pi-\pi$ packing and allows a good π-orbital overlap and a short centroid-to-centroid distance, thus enhancing the transfer integrals and the hopping

DOI: 10.1021/acs.chemmater.6b04277
Chem. Mater. XXXX, XXX, XXX−XXX

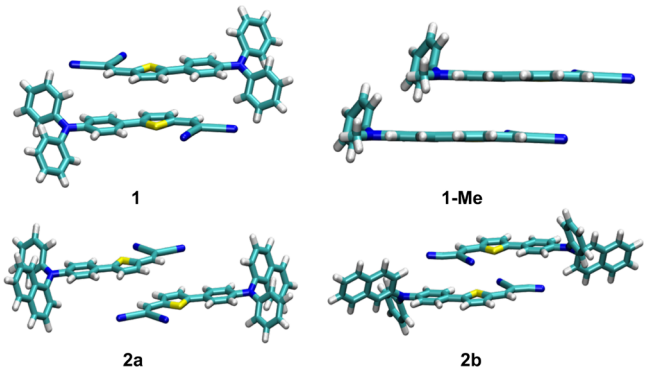

Figure 4. Main hopping pathway of hole transport in the investigated systems.

rates (see Table 6 and Figure 4). On the other hand, in **1** and **2a**, the crystal packing forces the conjugated rings to a more tilted configuration and increases the distance between the centroids, thus negatively affecting the orbital overlap and the transport properties. Notably, there is a sensible difference in the calculated hole mobility between **2a** and **2b**. These two compounds both present a naphthyl group but a different connectivity. The β-naphthyl compound (**2b**) shows a geometry more coplanar than that of the α-naphthyl one (**2a**) that leads to a higher hole mobility. This is related to the larger steric hindrance of the α-naphthyl group that generates a more twisted structure, negatively affecting the transport properties.

In the case of the four HTMs in the amorphous phase, for each system we calculated the hole mobility for 1000 configurations extracted from the MD simulations as described in Computational Methods. The calculations were repeated by applying an electric field of 10^6 V/m in several directions and averaging the resulting mobility values (μ_{amo}). The results are reported in Table 7.

Table 7. Hole Mobilities Calculated in the Amorphous Systems (μ_{amo}, in square centimeters per volt per second)

system	μ_{amo}
1	$(8.14 \pm 3.93) \times 10^{-11}$
1-Me	$(3.13 \pm 1.31) \times 10^{-11}$
2a	$(2.21 \pm 1.47) \times 10^{-11}$
2b	$(1.73 \pm 0.69) \times 10^{-10}$

The analyzed systems show similar low mobilities indicating a similar degree of local order in the amorphous phase. This is clearly evident from the calculation of the radial distribution function of the nitrogen atom belonging to the triphenylamine groups reported in Figure 5.

The radial distribution function is defined as the ratio[55,71]

$$g(r) = N(r)/g_I(r) \quad (7)$$

where $N(r)$ is the number of occurrences of radial distance r between pairs of particles and $g_I(r)$ is the radial distribution function of an ideal gas with density ρ [$g_I(r) = 4\pi\rho r^2$]. Using this type of normalization, $g(r \to \infty) = 1$. The presence of peaks in $g(r)$ would reveal the presence of ordered structures in the bulk.

Figure 5 shows a similar $g(r)$ for all the investigated systems: the differences in terms of molecular structure among the four molecules are too small to significantly influence the local order

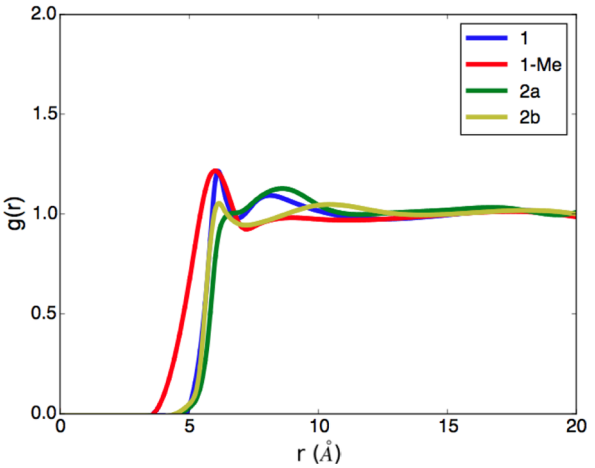

Figure 5. Radial distribution functions $g(r)$ of the nitrogen atom belonging to the triphenylamine groups of the simulated systems calculated from the MD trajectories in the amorphous phase.

properties of the amorphous bulks. Their similar low mobility values suggest that the amorphous domains of a typically polycrystalline HTM layer of a solar cell affect in analogous fashion the overall performance of the device.

Taken together, these results suggest that small modifications in the molecular structure of triphenylamine-based HTMs are able to strongly affect their transport properties in the crystalline phase. Importantly, our calculations show that the substitution of a phenyl in the triphenylamine unit does not significantly alter the electronic and optical properties of these materials. On the other hand, the tiny alteration of the molecular scaffold has a large effect on the molecular packing in the crystal structure. In particular, we show that the substitution of the phenyl with a methyl in **1-Me** enhances the face-to-face $\pi-\pi$ packing in the crystal structure, increasing the effective π-orbital overlap and thus increasing the hole mobility between conjugated molecules (see Table 6 and Figure 4). Moreover, we show that the molecular modifications do not alter significantly the low hole mobility of these materials in the bulk amorphous phase that is completely disordered for all systems.

The theoretical results, in agreement with the experimental findings,[32,34] indicate that to improve the transport properties and, consequently, the performance of a solar cell it is important to focus on the crystal phase of the HTM materials in designing molecules that can achieve the most suitable molecular packing for transport.

CONCLUSIONS

In this study, we theoretically investigate the effects of small molecular substitutions in the structure of triphenylamine-based hole transporter materials used in organic solar cells on their transport properties in the crystalline and amorphous phases. Exploiting DFT, TD-DFT, MD, and Marcus theory, we analyze the molecular rationale that lies behind the different measured transport properties of four HTMs whose scaffold differs only in the substitution of one phenyl ring in the triphenylamine unit. Our calculations clearly show that the effect of the substituents on the electronic and optical properties of these materials is negligible. On the other hand, chemical modifications have important effects on the molecular packing in the crystalline structure that can account for the

DOI: 10.1021/acs.chemmater.6b04277
Chem. Mater. XXXX, XXX, XXX−XXX

different calculated transport properties. In particular, we show that the substitution of the phenyl with a methyl in **1-Me** enhances the face-to-face $\pi-\pi$ packing in the crystal structure that allows a good π-orbital overlap at short centroid-to-centroid distances, enhancing the transfer integrals and the hopping rates. On the other hand, the presence of an α-naphthyl in **2a** generates a twisted structure due to the steric hindrance that negatively affects its transport properties.

Moreover, we find that the difference in the molecular structure of the four molecules is too small to significantly influence the degree of local order in the amorphous bulks all characterized by a completely disordered morphology and low mobilities. In fact, the amorphous phase is more sensitive to the overall shape of the molecules than to the effective chemical substitutions. In the case of the materials studied in this work, the modification of the molecular shape is too slight to affect the amorphous phase.

These results, in line with the experimental findings, suggest that in the quest for new performing materials that can improve the performance of a solar cell it is desirable to devise a strategy that, starting from small transformations of a molecular scaffold, leads to the optimization of the packing properties in the crystal phase and, consequently, to improved transport properties and more efficient solar cells.

■ ASSOCIATED CONTENT

Supporting Information

The Supporting Information is available free of charge on the ACS Publications website at DOI: 10.1021/acs.chemmater.6b04277.

Volume convergence plot (PDF)

■ AUTHOR INFORMATION

Corresponding Authors

*E-mail: jeanroncali@gmail.com.

*E-mail: carlo.adamo@chimie-paristech.fr.

ORCID

Alfonso Pedone: 0000-0003-3772-7222

Gianluca Lattanzi: 0000-0002-0808-6457

Carlo Adamo: 0000-0002-2638-2735

Notes

The authors declare no competing financial interest.

■ ACKNOWLEDGMENTS

We acknowledge CINECA Awards HP10CAJ6KE and HP10BWMW76 under the ISCRA initiative for the availability of high-performance computing resources and support.

■ REFERENCES

(1) Brabec, C.; Scherf, U.; Dyakonov, V. *Organic Photovoltaics: Materials, Device Physics, and Manufacturing Technologies*; John Wiley & Sons: New York, 2011.

(2) Günes, S.; Neugebauer, H.; Sariciftci, N. S. Conjugated Polymer-Based Organic Solar Cells. *Chem. Rev.* **2007**, *107*, 1324−1338.

(3) Cao, W.; Xue, J. Recent Progress in Organic Photovoltaics: Device Architecture and Optical Design. *Energy Environ. Sci.* **2014**, *7*, 2123−2144.

(4) Mazzio, K. A.; Luscombe, C. K. The Future of Organic Photovoltaics. *Chem. Soc. Rev.* **2015**, *44*, 78−90.

(5) Tang, C. W. Two-layer Organic Photovoltaic Cell. *Appl. Phys. Lett.* **1986**, *48*, 183−185.

(6) Kaur, N.; Singh, M.; Pathak, D.; Wagner, T.; Nunzi, J. Organic Materials for Photovoltaic Applications: Review and Mechanism. *Synth. Met.* **2014**, *190*, 20−26.

(7) Wöhrle, D.; Meissner, D. Organic Solar Cells. *Adv. Mater.* **1991**, *3*, 129−138.

(8) Peumans, P.; Yakimov, A.; Forrest, S. R. Small Molecular Weight Organic Thin-Film Photodetectors and Solar Cells. *J. Appl. Phys.* **2003**, *93*, 3693−3723.

(9) Yu, G.; Gao, J.; Hummelen, J. C.; Wudl, F.; Heeger, A. J. Polymer Photovoltaic Cells: Enhanced Efficiencies via a Network of Internal Donor-Acceptor Heterojunctions. *Science* **1995**, *270*, 1789−1791.

(10) Halls, J. J. M.; Walsh, C. A.; Greenham, N. C.; Marseglia, E. A.; Friend, R. H.; Moratti, S. C.; Holmes, A. B. Efficient Photodiodes from Interpenetrating Polymer Networks. *Nature* **1995**, *376*, 498−500.

(11) Cheng, Y.-J.; Yang, S.-H.; Hsu, C.-S. Synthesis of Conjugated Polymers for Organic Solar Cell Applications. *Chem. Rev.* **2009**, *109*, 5868−5923.

(12) Roncali, J. Molecular Bulk Heterojunctions: An Emerging Approach to Organic Solar Cells. *Acc. Chem. Res.* **2009**, *42*, 1719−1730.

(13) Li, Y.; Guo, Q.; Li, Z.; Pei, J.; Tian, W. Solution Processable D−A Small Molecules for Bulk-heterojunction Solar Cells. *Energy Environ. Sci.* **2010**, *3*, 1427−1436.

(14) Walker, B.; Kim, C.; Nguyen, T.-Q. Small Molecule Solution-Processed Bulk Heterojunction Solar Cells †. *Chem. Mater.* **2011**, *23*, 470−482.

(15) Mishra, A.; Bäuerle, P. Small Molecule Organic Semiconductors on the Move: Promises for Future Solar Energy Technology. *Angew. Chem., Int. Ed.* **2012**, *51*, 2020−2067.

(16) Lin, Y.; Li, Y.; Zhan, X. Small Molecule Semiconductors for High-efficiency Organic Photovoltaics. *Chem. Soc. Rev.* **2012**, *41*, 4245−4272.

(17) Kan, B.; Zhang, Q.; Li, M.; Wan, X.; Ni, W.; Long, G.; Wang, Y.; Yang, X.; Feng, H.; Chen, Y. Solution-Processed Organic Solar Cells Based on Dialkylthiol-Substituted Benzodithiophene Unit with Efficiency Near 10%. *J. Am. Chem. Soc.* **2014**, *136*, 15529−15532.

(18) Po, R.; Roncali, J. Beyond Efficiency: Scalability of Molecular Donor Materials for Organic Photovoltaics. *J. Mater. Chem. C* **2016**, *4*, 3677−3685.

(19) Bui, T.-T.; Goubard, F. Recent Advances in Small Molecular, Non-Polymeric Organic Hole Transporting Materials for Solid-State DSSC. *EPJ Photovoltaics* **2013**, *4*, 40402.

(20) Beaujuge, P. M.; Fréchet, J. M. J. Molecular Design and Ordering Effects in π- Functional Materials for Transistor and Solar Cell Applications. *J. Am. Chem. Soc.* **2011**, *133*, 20009−20029.

(21) Leliège, A.; Régent, C.-H. L.; Allain, M.; Blanchard, P.; Roncali, J. Structural Modulation of Internal Charge Transfer in Small Molecular Donors for Organic Solar Cells. *Chem. Commun.* **2012**, *48*, 8907−8909.

(22) Inostroza, N.; Mendizabal, F.; Arratia-Pérez, R.; Orellana, C.; Linares-Flores, C. Improvement of Photovoltaic Performance by Substituent Effect of Donor and Acceptor Structure of TPA-Based Dye-Sensitized Solar Cells. *J. Mol. Model.* **2016**, *22*, 25.

(23) Roncali, J.; Leriche, P.; Blanchard, P. Molecular Materials for Organic Photovoltaics: Small is Beautiful. *Adv. Mater.* **2014**, *26*, 3821−3838.

(24) Demeter, D.; Mohamed, S.; Diac, A.; Grosu, I.; Roncali, J. Small Molecular Donors for Organic Solar Cells Obtained by Simple and Clean Synthesis. *ChemSusChem* **2014**, *7*, 1046−1050.

(25) Zhang, X.; Grätzel, M.; Hua, J. Donor Design and Modification Strategies of Metal Free Sensitizers for Highly-Efficient n-type Dye-Sensitized Solar Cells. *Front. Optoelec.* **2016**, *9*, 3−37.

(26) Mahmood, A. Triphenylamine Based Dyes for Dye Sensitized Solar Cells: A review. *Sol. Energy* **2016**, *123*, 127−144.

(27) Quinton, C.; Alain-Rizzo, V.; Dumas-Verdes, C.; Clavier, G.; Vignau, L.; Audebert, P. Triphenylamine/tetrazine Based π-Conjugated Systems as Molecular Donors for Organic Solar Cells. *New J. Chem.* **2015**, *39*, 9700−9713.

DOI: 10.1021/acs.chemmater.6b04277
Chem. Mater. XXXX, XXX, XXX−XXX

(28) Yen, Y.-S.; Chou, H.-H.; Chen, Y.-C.; Hsu, C.-Y.; Lin, J. T. Recent Developments in Molecule-Based Organic Materials for Dye-Sensitized Solar Cells. *J. Mater. Chem.* **2012**, *22*, 8734−8747.
(29) Liang, M.; Chen, J. Arylamine Organic Dyes for Dye-Sensitized Solar Cells. *Chem. Soc. Rev.* **2013**, *42*, 3453−3488.
(30) Roquet, S.; Cravino, A.; Leriche, P.; Alévêque, O.; Frère, P.; Roncali, J. Triphenylamine-Thienylenevinylene Hybrid Systems with Internal Charge Transfer as Donor Materials for Heterojunction Solar Cells. *J. Am. Chem. Soc.* **2006**, *128*, 3459−3466.
(31) Luponosov, Y. N.; Solodukhin, A. N.; Ponomarenko, S. A. Branched Triphenylamine-Based Oligomers for Organic Electronics. *Polym. Sci., Ser. C* **2014**, *56*, 104−134.
(32) Jiang, Y.; Cabanetos, C.; Allain, M.; Liu, P.; Roncali, J. Manipulation of the Band Gap and Efficiency of a Minimalist Push−Pull Molecular Donor for Organic Solar Cells. *J. Mater. Chem. C* **2015**, *3*, 5145−5151.
(33) Leliège, A.; Grolleau, J.; Allain, M.; Blanchard, P.; Demeter, D.; Rousseau, T.; Roncali, J. Small D-π-A Systems with o-Phenylene-Bridged Accepting Units as Active Materials for Organic Photovoltaics. *Chem. - Eur. J.* **2013**, *19*, 9948−9960.
(34) Mohamed, S.; Demeter, D.; Laffitte, J.-A.; Blanchard, P.; Roncali, J. Structure properties Relationships in Triarylamine-Based Donor-Acceptor Molecules Containing Naphthyl Groups as Donor Material for Organic Solar Cells. *Sci. Rep.* **2015**, *5*, 9031.
(35) Chi, W.-J.; Li, Z.-S. The Theoretical Investigation on the 4-(4-phenyl-4-α-naphthylbutadieny)-triphenylamine Derivatives as Hole Transporting Materials for Perovskite-Type Solar Cells. *Phys. Chem. Chem. Phys.* **2015**, *17*, 5991−5998.
(36) Alberga, D.; Mangiatordi, G. F.; Labat, F.; Ciofini, I.; Nicolotti, O.; Lattanzi, G.; Adamo, C. Theoretical Investigation of Hole Transporter Materials for Energy Devices. *J. Phys. Chem. C* **2015**, *119*, 23890−23898.
(37) Yang, X.; Li, Q.; Shuai, Z. Theoretical Modelling of Carrier Transports in Molecular Semiconductors: Molecular Design of Triphenylamine Dimer Systems. *Nanotechnology* **2007**, *18*, 424029.
(38) Morvillo, P.; Bobeico, E. Tuning the LUMO Level of the Acceptor to Increase the Open-Circuit Voltage of Polymer-Fullerene Solar Cells: A Quantum Chemical Study. *Sol. Energy Mater. Sol. Cells* **2008**, *92*, 1192−1198.
(39) Alberga, D.; Perrier, A.; Ciofini, I.; Mangiatordi, G. F.; Lattanzi, G.; Adamo, C. Morphological and Charge Transport Properties of Amorphous and Crystalline P3HT and PBTTT: Insights From Theory. *Phys. Chem. Chem. Phys.* **2015**, *17*, 18742−18750.
(40) Zhang, L.; Shen, W.; He, R.; Liu, X.; Tang, X.; Yang, Y.; Li, M. Fine Structural Tuning of Diketopyrrolopyrrole-Cored Donor Materials for Small Molecule-Fullerene Organic Solar Cells: A Theoretical Study. *Org. Electron.* **2016**, *32*, 134−144.
(41) Zhang, L.; Shen, W.; He, R.; Tang, X.; Yang, Y.; Li, M. Density Functional Study on The Effect of Aromatic Rings Flanked by Bithiophene of Novel Electron Donors in Small-molecule Organic Solar Cells. *Mater. Chem. Phys.* **2016**, *175*, 13−21.
(42) Marcus, R. A. Electron Transfer Reactions in Chemistry. Theory and Experiment. *Rev. Mod. Phys.* **1993**, *65*, 599−610.
(43) Rühle, V.; Lukyanov, A.; May, F.; Schrader, M.; Vehoff, T.; Kirkpatrick, J.; Baumeier, B.; Andrienko, D. Microscopic Simulations of Charge Transport in Disordered Organic Semiconductors. *J. Chem. Theory Comput.* **2011**, *7*, 3335−3345.
(44) Stehr, V.; Fink, R. F.; Engels, B.; Pflaum, J.; Deibel, C. Singlet Exciton Diffusion in Organic Crystals Based on Marcus Transfer Rates. *J. Chem. Theory Comput.* **2014**, *10*, 1242−1255.
(45) Kirkpatrick, J. An Approximate Method for Calculating Transfer Integrals Based on the ZINDO Hamiltonian. *Int. J. Quantum Chem.* **2008**, *108*, 51−56.
(46) Baumeier, B.; Kirkpatrick, J.; Andrienko, D. Density-functional Based Determination of Intermolecular Charge Transfer Properties for Large-Scale Morphologies. *Phys. Chem. Chem. Phys.* **2010**, *12*, 11103−11113.
(47) Poelking, C.; Andrienko, D. Effect of Polymorphism, Regioregularity and Paracrystallinity on Charge Transport in Poly(3-hexylthiophene) [P3HT] Nanofibers. *Macromolecules* **2013**, *46*, 8941−8956.
(48) Poelking, C.; Cho, E.; Malafeev, A.; Ivanov, V.; Kremer, K.; Risko, C.; Brédas, J.-L.; Andrienko, D. Characterization of Charge-Carrier Transport in Semicrystalline Polymers: Electronic Couplings, Site Energies, and Charge-Carrier Dynamics in Poly(bithiophene- alt -thienothiophene) [PBTTT]. *J. Phys. Chem. C* **2013**, *117*, 1633−1640.
(49) Yavuz, I.; Martin, B. N.; Park, J.; Houk, K. N. Theoretical Study of the Molecular Ordering, Paracrystallinity, And Charge Mobilities of Oligomers in Different Crystalline Phases. *J. Am. Chem. Soc.* **2015**, *137*, 2856−2866.
(50) *Materials Studio*; Accelrys: San Diego, 2005.
(51) Perdew, J. P.; Burke, K.; Ernzerhof, M. Generalized Gradient Approximation Made Simple. *Phys. Rev. Lett.* **1996**, *77*, 3865−3868.
(52) Mayo, S. L.; Olafson, B. D.; Goddard, W. A. DREIDING: a Generic Force Field for Molecular Simulations. *J. Phys. Chem.* **1990**, *94*, 8897−8909.
(53) Sokolov, A. N.; Atahan-Evrenk, S.; Mondal, R.; Akkerman, H. B.; Sánchez-Carrera, R. S.; Granados-Focil, S.; Schrier, J.; Mannsfeld, S. C.; Zoombelt, A. P.; Bao, Z.; Aspuru-Guzik, A. From Computational Discovery to Experimental Characterization of a High Hole Mobility Organic Crystal. *Nat. Commun.* **2011**, *2*, 437.
(54) Zhang, B.; Kan, Y.-H.; Geng, Y.; Duan, Y.-A.; Li, H.-B.; Hua, J.; Su, Z.-M. An Efficient Strategy for Improving Carrier Transport Performance − Introducing Fluorine Into Aryl Substituted Tetracene. *Org. Electron.* **2013**, *14*, 1359−1369.
(55) Alberga, D.; Mangiatordi, G. F.; Torsi, L.; Lattanzi, G. Effects of Annealing and Residual Solvents on Amorphous P3HT and PBTTT Films. *J. Phys. Chem. C* **2014**, *118*, 8641−8655.
(56) Phillips, J. C.; Braun, R.; Wang, W.; Gumbart, J.; Tajkhorshid, E.; Villa, E.; Chipot, C.; Skeel, R. D.; Kalé, L.; Schulten, K. Scalable Molecular Dynamics with NAMD. *J. Comput. Chem.* **2005**, *26*, 1781−1802.
(57) Vanommeslaeghe, K.; Hatcher, E.; Acharya, C.; Kundu, S.; Zhong, S.; Shim, J.; Darian, E.; Guvench, O.; Lopes, P.; Vorobyov, I.; Mackerell, A. D. CHARMM General Force Field: A Force Field for Drug-Like Molecules Compatible with the CHARMM All-Atom Additive Biological Force Fields. *J. Comput. Chem.* **2009**, 671−690.
(58) Yu, W.; He, X.; Vanommeslaeghe, K.; MacKerell, A. D. Extension of the CHARMM General Force Field to Sulfonyl-Containing Compounds and its Utility in Biomolecular Simulations. *J. Comput. Chem.* **2012**, *33*, 2451−2468.
(59) Bayly, C. I.; Cieplak, P.; Cornell, W.; Kollman, P. A. A Well-Behaved Electrostatic Potential Based Method Using Charge Restraints for Deriving Atomic Charges: the RESP Model. *J. Phys. Chem.* **1993**, *97*, 10269−10280.
(60) Coropceanu, V.; Cornil, J.; da Silva Filho, D. A.; Olivier, Y.; Silbey, R.; Brédas, J.-L. Charge Transport in Organic Semiconductors. *Chem. Rev.* **2007**, *107*, 926−952.
(61) Besler, B. H.; Merz, K. M.; Kollman, P. A. Atomic Charges Derived from Semiempirical Methods. *J. Comput. Chem.* **1990**, *11*, 431−439.
(62) Malagoli, M.; Coropceanu, V.; da Silva Filho, D. A.; Brédas, J. L. A Multimode Analysis of the Gas-Phase Photoelectron Spectra in Oligoacenes. *J. Chem. Phys.* **2004**, *120*, 7490.
(63) Rosso, K. M.; Dupuis, M. Electron Transfer in Environmental Systems: a Frontier for Theoretical Chemistry. *Theor. Chem. Acc.* **2006**, *116*, 124−136.
(64) Sánchez-Carrera, R. S.; Coropceanu, V.; da Silva Filho, D. A.; Friedlein, R.; Osikowicz, W.; Murdey, R.; Suess, C.; Salaneck, W. R.; Brédas, J.-L. Vibronic Coupling in the Ground and Excited States of Oligoacene Cations. *J. Phys. Chem. B* **2006**, *110*, 18904−18911.
(65) Stehr, V.; Engels, B.; Deibel, C.; Fink, R. F. Anisotropy of Singlet Exciton Diffusion in Organic Semiconductor Crystals From Ab Initio Approaches. *J. Chem. Phys.* **2014**, *140*, 024503.
(66) Fink, R. F.; Pfister, J.; Zhao, H. M.; Engels, B. Assessment of Quantum Chemical Methods and Basis Sets for Excitation Energy Transfer. *Chem. Phys.* **2008**, *346*, 275−285.

DOI: 10.1021/acs.chemmater.6b04277
Chem. Mater. XXXX, XXX, XXX−XXX

(67) Davydov, A. S. The Theory of Molecular Excitons. *Sov. Phys. Usp.* **1964**, *7*, 145−178.
(68) Tomasi, J.; Mennucci, B.; Cammi, R. Quantum Mechanical Continuum Solvation Models. *Chem. Rev.* **2005**, *105*, 2999−3094.
(69) Song, Y.; Lv, S.; Liu, X.; Li, X.; Wang, S.; Wei, H.; Li, D.; Xiao, Y.; Meng, Q. Energy Level Tuning of TPB-Based Hole-Transporting Materials for Highly Efficient Perovskite Solar Cells. *Chem. Commun.* **2014**, *50*, 15239−15242.
(70) Scholes, G. D.; Rumbles, G. Excitons in Nanoscale Systems. *Nat. Mater.* **2006**, *5*, 683−696.
(71) Alberga, D.; Mangiatordi, G. F.; Motta, A.; Nicolotti, O.; Lattanzi, G. Effects of Different Self-Assembled Monolayers on Thin-Film Morphology: A Combined DFT/MD Simulation Protocol. *Langmuir* **2015**, *31*, 10693−10701.

DOI: 10.1021/acs.chemmater.6b04277
Chem. Mater. XXXX, XXX, XXX−XXX